



ORIGINAL ARTICLE

Push-out tests: connections by adherence in the context of latticed joist slabs

Ensaio de push-out: conexões por aderência no contexto de lajes treliçadas

Lisarb Henneh Brasil^a Hidelbrando José Farkat Diógenes^a Maria Isabel Brito Valente^b Lays Raianne Azevedo da Costa^a ^aUniversidade Federal da Paraíba – UFPB, Civil and Environment Engineering Department, João Pessoa, PB, Brasil^bUniversidade do Minho – Uminho, Department of Civil Engineering, Guimarães, Portugal

Received 19 July 2023

Accepted 21 November 2023

Abstract: Composite structures and precast solutions stand out because they lead to simple, fast erected and economic constructions. In steel-concrete composite construction, shear connectors are used to assure the shear transfer between the steel profile and the concrete slab, enabling the composite action to develop. This paper discusses an innovative technology for connection by adherence, whose resistance is due to friction on various steel-concrete interfaces. The authors consider that this type of shear connection is suitable for composite beams with latticed joists slabs, and the study developed intends to analyze the behavior of the proposed connection, in this application's context, through experimental and numerical approaches. For this purpose, push-out specimens were fabricated and tested in accordance with Eurocode-4 requirements, where the connection behavior is analyzed in terms of its load-slip relation, and the failure modes are identified. Experimental and numerical results allowed to induce that the connector by adherence made with a checkered steel plate is appropriate to be used in composite structures, as it exhibits satisfactory shear resistance and ductility performance. Also, specimens with latticed joist slabs presented average load capacity values with the same magnitude as the average load capacity obtained in models with solid slabs, despite being more prone to cracking. From the parametric study, an increase of 100% in the connector height implied strength increase from 16% to 25%, depending on slab type.

Keywords: prefabricated structures, rib connectors, push-out test, finite element analysis.

Resumo: As estruturas mistas e as soluções pré-moldadas se destacam por possibilitarem construções simples, rápidas e econômicas. Em construções mistas de aço-concreto, são utilizados conectores de cisalhamento para garantir a transferência de cisalhamento entre o perfil de aço e a laje de concreto, permitindo o desenvolvimento da ação mista. Este trabalho aborda uma tecnologia inovadora de ligação por aderência, cuja resistência se dá por atrito em diversas interfaces aço-concreto. Os autores consideram que este tipo de ligação é adequado para vigas mistas com lajes treliçadas, e o estudo desenvolvido pretende analisar o comportamento da ligação proposta, no contexto desta aplicação, através de abordagens experimentais e numéricas. Para atingir os objetivos propostos, corpos-de-prova de push-out foram produzidos e ensaiados de acordo com os requisitos do Eurocode-4, onde o comportamento da ligação foi analisado em termos da sua relação carga-escorregamento e foram identificados os modos de falha. Resultados experimentais e numéricos permitiram induzir que o conector por aderência produzido com chapa de aço do tipo xadrez é adequado para ser utilizado em estruturas mistas, pois apresenta desempenho satisfatório de resistência ao cisalhamento e ductilidade. Além disso, os corpos-de-prova com lajes treliçadas apresentaram valores médios de capacidade de carga com a mesma magnitude que a média de capacidade de carga obtida em modelos com lajes maciças, apesar de serem mais propensos a fissuração. Pelo estudo paramétrico, um aumento de 100% na altura do conector implicou ganho de resistência de 16% a 25%, dependendo do tipo de laje.

Palavras-chave: estruturas pré-fabricadas, conectores de pino, ensaios de push-out, análise por elementos finitos.

How to cite: L. H. Brasil, H. J. F. Diógenes, M. I. B. Valente, and L. R. A. Costa, "Push-out tests: connections by adherence in the context of latticed joist slabs," *Rev. IBRACON Estrut. Mater.*, vol. 17, no. 6, e17602, 2024, <https://doi.org/10.1590/S1983-41952024000600002>

Corresponding author: Hidelbrando José Farkat Diógenes. E-mail: hjfd@academico.ufpb.br

Financial support: The authors declare that during the preparation of this manuscript funds were received from the Coordination for the Improvement of Higher Education Personnel (CAPES) and the National Council for Scientific and Technological Development (CNPq). In addition a donation of RC steel bars and metal profiles were received from Gerdaul S.A and J.C. Metallurgy, respectively.

Conflict of interest: The authors declare that they have no known competing financial interests or personal relationships that could have appeared to influence the work reported in this paper.

Data Availability: The data that support the findings of this study are available from the corresponding author, HJFD, upon reasonable request.



This is an Open Access article distributed under the terms of the Creative Commons Attribution License, which permits unrestricted use, distribution, and reproduction in any medium, provided the original work is properly cited.

1 INTRODUCTION

Steel and concrete composite structures combine the favorable properties of both materials, ideally by positioning the concrete in the compression zone and the steel in the tensile zone. This type of composite structures has been extensively applied to bridges and buildings due to their excellent performance and economy, where the steel frame provides great ease of installation, and concrete provides useful strength at low cost [1], [2]. An adequate shear transfer is always desirable to ensure the composite action, which can be obtained by means of shear connector to reduce or preventing the relative displacement of steel and concrete sections at their interface [3]. Previous studies indicate that headed stud is the most common type of mechanical shear connector, particularly in prefabricated structures, but this connector favor cracks formation which slows down the connection durability, because they act as singularities that can create stress concentration [4]. But the development of new types of connectors as in Bouazaoui et al. [5], Thomann and Lebet [6] and Alves et al. [7] seeks to overcome these disadvantages, because linear or surface connections are developed, rather than point connections, keeping the stress concentration as small as possible.

Several authors studied the behavior of Perfobond connectors specifically by the evaluation of results obtained in push-out tests or by the development of numerical models. It was concluded that their structural response is influenced by several parameters, such as the number of holes, width, length, and thickness of the rib, the tensile strength of the concrete slab along the Perfobond alignment, presence and percentage of transverse reinforcement bars in the concrete slab, shear resistance of the confined concrete inside the connector's openings and bearing strength of the compressed concrete positioned in front of the Perfobond rib [8]–[13].

Connection by adherence initially studied by Thomann and Lebet [14] seems to be very promising in reducing the time of construction and improving the durability of the system without increasing the solution cost [15]. Connections by adherence advantages result from their resistance to shear, high stiffness in the initial phase of loading up to the maximum load capacity, and a high ductility guaranteed by a slight decrease of load capacity accompanied of high slip after the maximum load value [4], [6].

Two geometries of an embossed steel plate connector were studied and assessed by Diógenes et al. [15] the R type and the RP-type (Figure 1a and Figure 1b), to find shear connectors that are especially adequate for prefabricated elements and easy to assemble. Both the R-type and the RP-type connector received a mechanical treatment to create superficial grooves with 45° orientation, 2 mm depth, and 10 mm width. The innovative connector proposed comprises an embossed steel plate longitudinally welded to the steel girder's upper flange. In the present research, a linear connector formed by chess-type plates welded back-to-back was used (Figure 1c).

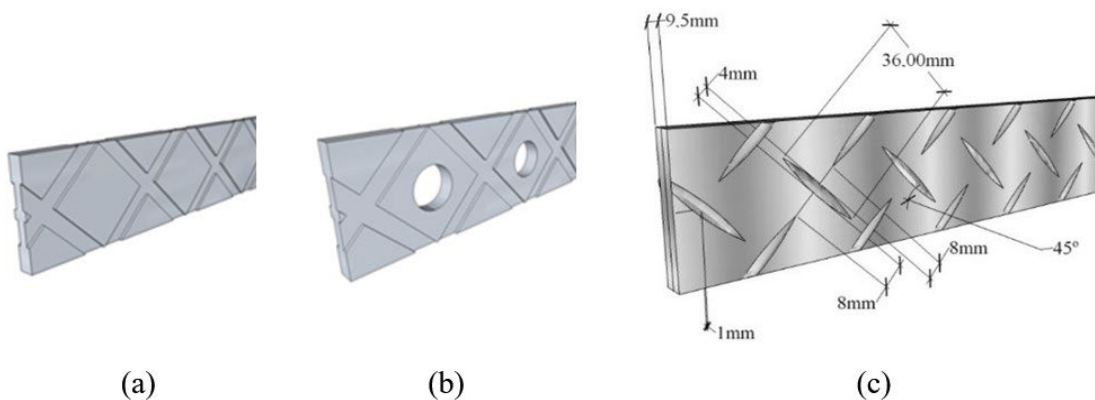


Figure 1. Linear connectors. A) R-type and (b) RP-type; (c) Checkered type plates welded “back-to-back”

The floor system with lattice joists, which is a type of ribbed slab, consisting of prefabricated slabs is a type of slab that is adequate for low and medium construction sites, and consists of a series of parallel reinforced concrete T beams framing into reinforced concrete girders. The ribs reinforcement is formed by the lattice joist. The main advantages of latticed joist slabs are the low volume of concrete, the reduced dead weight, and the improved formwork system for casting, facilitating assembly and streamlining work. The beams that support the latticed joists are usually made of reinforced concrete (see Figure 2a), but in this paper, a new solution is proposed, especially adequate for steel-framed buildings.

This paper addresses a new type of composite beam, composed of a steel inverted T section embedded in the concrete section, where the web is produced with checkered plates to guarantee the needed shear connection with the involving concrete section. The beam is then used to support the latticed joists, as represented in Figure 2b. This is a direct and practical application of the linear connections by adherence concept.

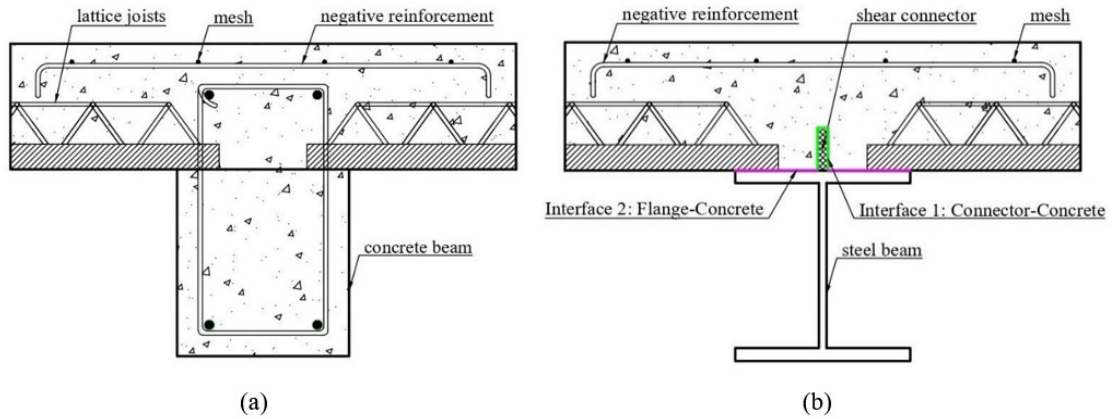


Figure 2. (a) Conventional floor system with lattice joists slab. (b) New proposed system for composite beam – Interfaces

This paper presents an experimental approach to assess the applicability of steel-concrete connection by adherence in building constructions, which promotes new knowledge on the topic. It is intended to evaluate this connector use specifically in the context of precast floor system with latticed joists, where connectors by adherence are part of the composite girder that gives support to the latticed joists. This solution takes advantage of the simplicity of erection, as the latticed joists are supported by the flange of the inverted T steel section. The structural behavior of the composite girder is also optimized, as the inverted T section is in the tensile part of the cross-section, and the concrete is on the compressed part of the cross-section.

The linear connector that is experimentally evaluated consists of a ribbed surface produced from a checkered steel plate. Push-out tests are performed to evaluate and discuss the structural behavior of this connection using linear connectors formed by ASTM – A36 checkered plates (Figure 1c). Additionally, the gaps in the experimental campaign are filled by a numerical model performed in Abaqus Simulia®. This plate typology was chosen because the authors believe that it can be efficiently used as a shear connector by adherence and is commercially available in many countries.

2 EXPERIMENTAL PROGRAM

Push-out tests were performed in the LABEME – Laboratory of Tests in Materials and Structures at the Federal University of Paraíba, Brazil, that were designed to study the interfaces involved in the proposed connection by adherence. The setup was designed to obtain the experimental response in terms of load and slip evolution, which can provide a criterion of the connection failure, and the slab uplift and slip behavior, which can translate a kinematic law that describes the prototype deformed configuration.

2.1 Specimen description

Six push-out prototypes were manufactured, based on recommendation of Eurocode 4 [16]. These specimens consisted of a steel beam positioned between two concrete slabs and connected to each of them by continuous ribbed steel plates that are longitudinally welded to the steel beam. The connector is longitudinally welded on the upper and bottom flanges of the steel beam and stays embedded in the concrete slab after concreting to ensure the connection between the steel beam and the concrete slab. Two different push-out specimens were designed to enable new discussions on Connection by Adherence. Three specimens use solid reinforced concrete slabs named MAC 1, MAC 2 and MAC 3, and three other models use latticed joist slabs called TREL 1, TREL 2 and TREL 3.

Two identical parts of the steel plate are welded in the back-to-back position to obtain the same pattern ribbed surface on both connector sides. Each checkered steel plate that composes the linear connector is 4.75 mm (3/16") thick, and therefore, the total thickness of the connector is 9.5 mm. The total length and height are 550 mm and 50 mm, respectively. The plate's surface has ribs of 1 mm depth with $\pm 45^\circ$ orientation, equally spaced and intercalated as a function of the direction (Figure 3).

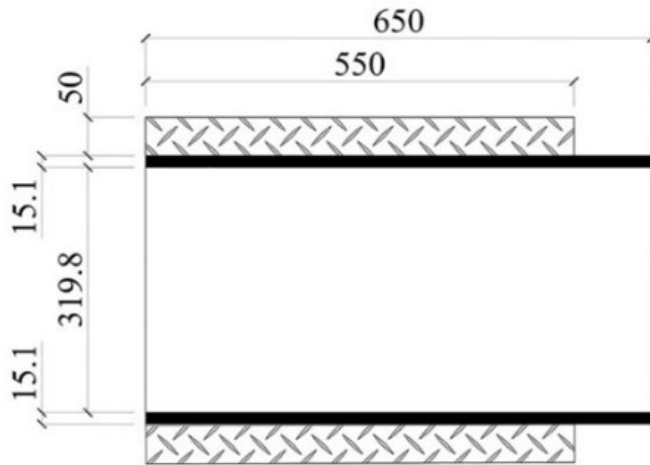


Figure 3. View of connector + Steel-based profile (unit:mm)

The steel profile used in the research corresponds to the W360x72 grade (ASTM-A572 grade 50), which is similar to the material characteristics proposed in Eurocode 4 [16] for push-out specimens. The shear connector is welded to the steel-based profile, as in Figure 3.

The first slab type is a reinforced concrete slab, where the rate and arrangement of the reinforcement is based on the Eurocode 4 [16] recommendations (Figure 4a). The second slab type, presented in Figure 4b, is a ribbed slab (similar to a precast ribbed slab made by lattice joist). The reinforcement arrangement differs according to the typology of the slabs, as shown in Figure 4. In the bulk reinforced concrete slab, the reinforcement consists of equally spaced steel CA-50 bars of 8 mm diameter. The reinforcement used in the ribbed slab specimens consists of TG8L – GERDAU® trusses with 8 cm of height, made by steel bars of 6.0 mm, 3.4 mm, and 4.2 mm diameter in the top flange, diagonals, and bottom flange, respectively. Also, an electro-welded mesh produced with CA-60 steel bars of 3.4 mm diameter, equally spaced of 15 cm in both directions, was used to prevent excessive cracking that results from loading and from concrete shrinkage.

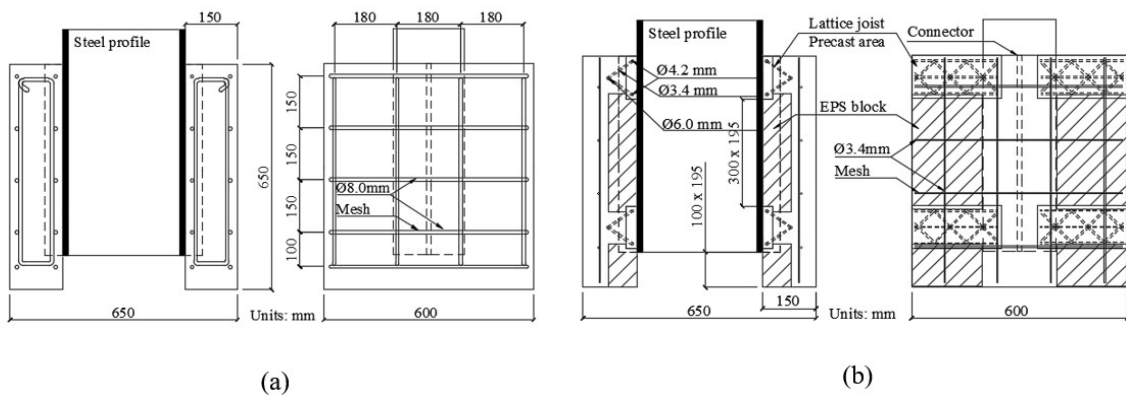


Figure 4. Specimens (a) MAC; (b) TREL

MAC and TREL specimens' transversal reinforcement area is $A_{s,MAC} = 2.51 \text{ cm}^2$ and $A_{s,TREL} = 0.36 \text{ cm}^2$. Thus, the ratio between the transversal reinforcement area and the concrete area is 0.36% for specimens with solid slab and 0.07% for models with lattice joists slab. Shear stresses will be developed along with the existent interfaces (see Figure 2b) to transmit the load from the steel element to the blocks of reinforced concrete, as well as by end-bearing resistance from the connector.

2.2 Materials' properties

Compressive strength and modulus of elasticity were determined using the recommendations of ABNT NBR 5739 [17] and ASTM-C215-08 [18]. Five concrete cylinders are tested for each casting. The concrete mixture (1:1,89:2,26:0,56) used for all specimens was: cement CII E-32, sand ($\Phi_{\text{máx}} = 4,75 \text{ mm}$), aggregates ($\Phi_{\text{máx}} = 12,5 \text{ mm}$); water/cement ratio 0,56. For concrete modulus of elasticity determination, nondestructive tests were carried out using the Sonelastic® software. The tension tests both connectors and steel profiles were following the dispositions defined in ABNT NBR 6152 [19]. For this, were used 3 samples of the checkered plate and 6 samples of the steel profile (3 for the web and 3 for the flange). Table 1 summarizes the mechanical properties obtained.

Table 1. Material Properties

CONCRETE			STEEL			
Specimen	$E_{\text{long,din}}$ (GPa)	f_{cm} (MPa)	Steel Type	E_{long} (GPa)	f_y (MPa)	f_u (MPa)
MAC-1	32.00	27.89	Beam Flange - ASTM A572 Grade 50	200.0 ^a	358.0	488.0
MAC-2	31.05	29.78				
MAC-3	30.11	33.85	Beam Web - ASTM A572 Grade 50	200.0 ^a	355.9	519.4
TREL-1	33.98	33.84				
TREL-2	32.23	32.34	Connector - ASTM A36		235.5	317.4
TREL-3	32.04	24.71				
Mean	31.90	30.40				

^a Nominal value of modulus of elasticity.

2.3 Test setup and loading procedure

According to Eurocode 4 [16], monotonic and cyclic tests were carried out to evaluate the ultimate strength of the shear connection, to obtain the complete load-slip curve, and to analyze the relation between uplift and slip. The loading procedure included the force-controlled cyclic pre-loading steps and the monotonic loading step. In the pre-loading steps, the load ranged from 5% to 40% of the estimated ultimate load, according to Annex B of Eurocode 4 [16] and based on the mean' ultimate load obtained by Diógenes et al. [15], that was 585.5kN. The test was divided into four distinct phases to better evaluate the behavior of the specimen. As the load magnitude in the initial three phases is relatively small compared to the peak load, a small slip, uplift, or cracking is expected. For this reason, a load application rate of 1.0 kN/s was adopted. In the following phases, the load application rate was reduced to 0.5 kN/s.

Phase 1 consists of a pre-load of 20 kN. Phase 2 is characterized by cyclic loading, where 25 cycles of loading and ranging from 20 kN to 100 kN are applied at a speed of 1 kN/s and Phase 3 corresponds to a reload situation from 20 kN to 100 kN. To conclude, Phase 4 of the test is characterized by a continuous loading up to the specimen's failure, including the post-peak behavior, at a rate of 0.5 kN/s.

Six dial indicators (LCD) were used to monitor the test, two of these with a maximum range of 101.6 mm (4") and four with a maximum range of 25.4 mm (1"). A single linear variable displacement transducer (LVDT) with a maximum range of 25.4 mm (1") was also used (Figure 5). LCD-1, LCD-2, LCD-4, and LCD-5 dial indicators were installed at half the height of the model to measure the slip between the concrete block and the steel profile. As seen in Figure 5, each slab has two LCD's to present average slip results. LCD 3 and LCD 6 indicators were positioned between the two slabs in the upper region to measure the relative transverse displacement between them – uplift. The LVDT fixed in the upper part of slab 2 was used as a relative slip control device located directly on the connector.

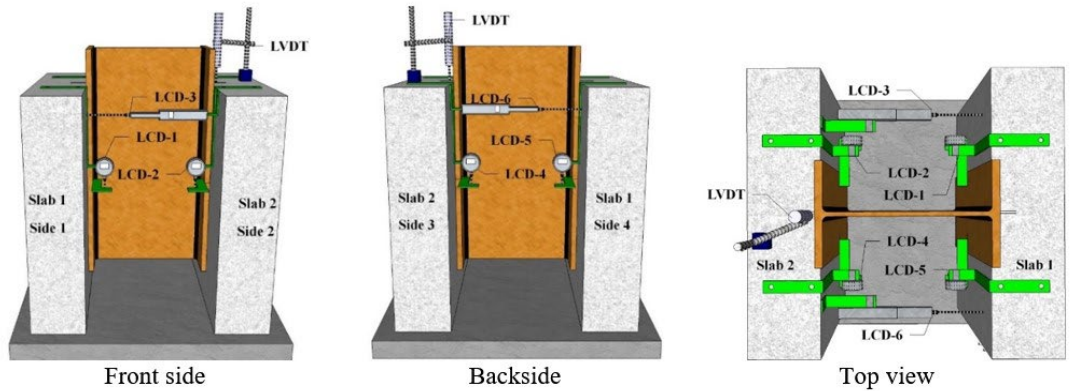


Figure 5. Instrumentation setup

2.4 Results and discussion

The discussions presented in this section refers to phase 4 of the test (monotonic test). Table 2 presents the results obtained for push-out tests: maximum load (P_{max}); slip referring to the maximum force ($\delta_{P_{max}}$); characteristic load corresponding to 90% of the maximum force (P_{Rk}); and characteristic slip (δ_{uk}); design value of bearing capacity (P_{Rd}); design slip (δ_d); shear stiffness per connector (K_s); and ductility factor (D_c). K_s is the slope of the line between the origin and P_{Rd} on load-slip curves and D_c is the ratio of δ_{uk} to $\delta_{P_{max}}$. The slip values presented are the average of value records obtained in LCD-1 to LCD-5. The results presented on Table 2 were extracted from each slab’s overall curves Figure 6, and based on standard values presented on Figure 6c.

2.4.1 Maximum load capacity

MAC specimens presented maximum load capacity values between 359.1 kN and 419.8 kN. TREL-1 and TREL-2 specimens presented maximum load capacity values of 409.2 kN and 357.2 kN, respectively. TREL-3 model presented a maximum load capacity of only 271.8 kN, which is considered atypical when compared to all other specimens. That phenomenon is explained by the very asymmetrical behavior of this specimen during the test, which failed on one side, while the other side remained almost intact, thus compromising the maximum strength of the specimen (Figure 10f), and so, the result of specimen TREL-3 was not considered. The MAC specimens present a slightly higher average value of maximum load capacity and lower variation when compared to the TREL specimens. MAC specimens reach, on average, a maximum load capacity of 393.5 kN while the TREL specimens reach 383.2 kN. The maximum load capacity registered on TREL specimens is around 97% of the corresponding value attained by MAC specimens.

Table 2. Main results for push-out tests.

Specimen	$P_{max,i}$ [kN]	$\delta_{P_{max,i}}$ [mm]	$P_{Rk,i}$ [kN]	$\delta_{uk,i}$ [mm]	P_{Rd} [kN]	δ_d [mm]	K_s [kN/mm]	D_c
MAC-1	359.1	2.02	323.2	5.47		0.15	861.8	2.70
MAC-2	417.2 ^a /419.8	2.01 ^a /4.50	375.4	7.90	258.5	0.21	615.6	3.93
MAC-3	404.3	2.57	363.9	8.41		0.16	807.9	3.27
TREL-1	409.2	2.40	368.3	7.00		0.48	267.9	2.91
TREL-2	357.2	2.89	321.5	4.01	257.2	0.27	476.3	1.38
TREL-3	271.8 ^b	1.86	244.6 ^b	3.94	-	-	-	2.11

^a Value adopted; ^b Value not considered

The values of maximum load (P_{max}) and corresponding slip ($\delta_{P_{max}}$) adopted for MAC-2 model refer to the first maximum load attained in this specimen, which is measured at the beginning of the constant load plateau that is developed before the descending branch. Thus, analyzes of stiffness and ductility become more coherent with the other specimens, MAC-1 and MAC-3. In terms of slip measured when the maximum load is applied, MAC specimens present an average value of 2.20 mm, while TREL specimens present 2.64 mm.

Figure 6 shows the behavior of the specimens tested to Load and corresponding Slip. Figure 6a refers to the evolution of the relationship between the parameters throughout the test, while Figure 6b represents the same curves but up to a maximum slip of 6 mm, where the models have already reached the maximum load capacity and are now at the beginning of descending branch of the load-slip curve. A straight vertical line was used to separate the ascending and descending branches from the corresponding curves.

It is possible to observe a similar behavior between all the MAC type specimens. They present an initial rigid behavior with very small values of slip ($\delta < 1$ mm) up to a load value that is around 90% of the maximum load capacity. After the maximum load is attained, the load capacity decreases slowly. For P_{Rk} (measured in the decreasing branch of the load slip curve), it is possible to measure slip values that are always higher than 5.47 mm.

MAC specimens show a gradual and continuous increase of deformation, from the instant of maximum load until the end of the test, except for the specimen MAC-1, which presents some residual stiffness, in which it reacquires some load capacity from 11 mm of slip on. This result is probably related to the activation of resistant mechanisms that are provided by the presence of reinforcement in the slab. The reinforcement in the slab increases the confining stresses on the connector and limits the crack opening [20].

In turn, TREL models present an initial behavior with very small values of slip ($\delta < 1$ mm) up to a load value that is around 70-80% of the maximum load capacity. Between around 70-80% and 100% of the maximum load capacity, larger slip values are registered and therefore, the stiffness of the connection is now smaller, as can be observed in Figure 6b. Upon reaching the maximum load, a rapid decrease in the load capacity of TREL-1 and TREL 2 models is observed, which continues until the end of the test. This fact characterizes a more premature rupture of these models and indicates a less ductile behavior when compared to the MAC Models. In TREL-3 specimen, the maximum load capacity was lower, so it was not possible to observe the rapid decrease of load capacity that occurred in specimens TREL-1 and TREL-2.

Indeed, the accentuation of the asymmetric behavior observed in the final phase of the TREL test motivated a unilateral mobilization of the model, contributing to the premature rupture. This rapid decrease of the load capacity in TREL specimens, after the maximum load is attained, also leads to smaller characteristic slip values (Figure 6).

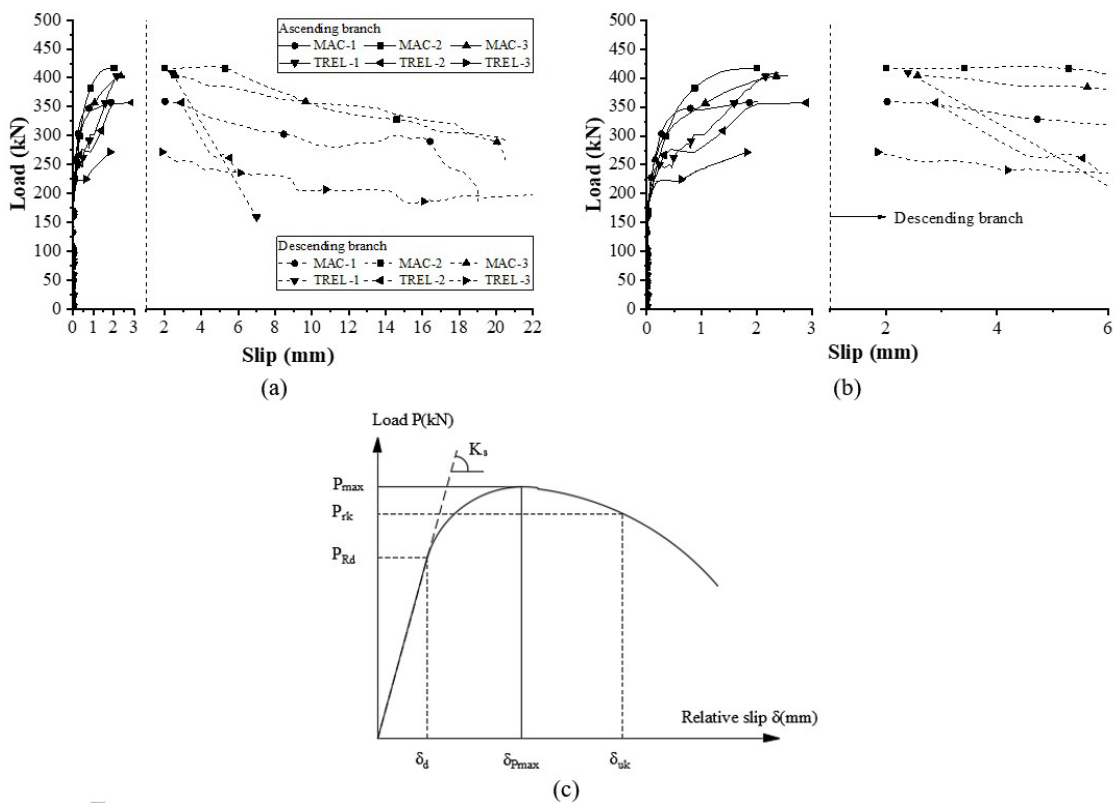


Figure 6. (a) Overall curves – Load \times Slip. (b) Zoom in early stages. (c) Standard Valeus

2.4.2 Failure modes

Two interfaces are involved in the Connection by Adherence proposed (see Figure 2b): Interface 01 — between the concrete slab and the shear connector, and Interface 02 — between the concrete slab and the steel flange. The mechanism of failure on these interfaces is due to the tensile stresses developed on the concrete slab under the effect of shear connector loading, leading to its progressive cracking. The concrete cracking allows the slip of the connector, which progressively imposes more damage to the concrete slab. At a certain point, the progressive cracking of the concrete slab leads to the decrease of the load-bearing capacity on the shear connector because the slab is not able to support the load that the connector is trying to transmit. The connector itself may present some linear deformation or warping in the lower region, which did not occur in this research, and the failure of the specimens was conditioned by the concrete slabs.

On connections by adherence, due the embossments on the interface, the slip is also accompanied by a separation of materials, called uplift, which is the transverse displacement of the concrete slab, perpendicularly to the shear loading direction. The combined effect of slip with uplift results in the interface's smoothing and contribute to the observed deformed model. The failure of Connection by Adherence does not occur with the beginning of slip. The failure modes related to Push Out tests were also discussed by Diógenes et al. [15], Kim et al. [21], Kim and Jeong [22], Jeong et al. [23] and Valente and Cruz [24].

2.4.3 MAC specimens

In MAC-1, the presence of the first cracks was observed in the region near the connector, at the top of slab 2, for a total load of 331.4 kN, that represents 92% of the maximum load capacity of this specimen. New cracks appeared on the inner side of slab 2, at the zone immediately below the connector, for a load of 347.0 kN (Figure 7a). MAC-1 reached a maximum load of 359.1 kN, when it was possible to observe a more significant opening of the existing cracks, especially in the inner region of slab 2. Afterwards, cracks began to appear aligned with the connector at the top of slab 1 (Figure 7b). As the test progressed, no new cracks appeared and there was propagation and opening of the existing cracks in the slabs' top (Figure 7b), as well as the progressive crushing of concrete in the inner region.

In MAC-2, the first cracks appeared simultaneously in the inner region of slabs 1 and 2, in the zone below the connector, for a load of 415.6 kN. At 417.2 kN, new cracks developed, aligned with the connector, this time at the top of both slabs. The first cracks occurred when the load value corresponded to more than 90% of the specimen's maximum load capacity, which is equal to 419.8 kN for MAC-2 specimen and was registered at 61 minutes of testing. Before the maximum load is attained, the development of cracks in the top of both slabs is observed and these propagate aligned with the shear connector (Figure 8c and Figure 8d).

When the maximum load is attained and until the end of the test, there is also a new longitudinal crack in the outer face of slab 1, aligned with the position of the shear connector, that develops from the bottom to the upper part of the slab (Figure 7c). At maximum load, the cracks in the inner region of the slabs have already developed significantly, leading to the crushing of concrete in that region (Figure 7d). MAC-3 specimen presented an experimental behavior similar to MAC-2 regarding the sequence of cracking: a) the appearance of the first cracks occurred at a load corresponding to 82% of the maximum load specimen' capacity, to a load value of 335.3 kN; b) there were no longitudinal cracks in the outer slabs' face.

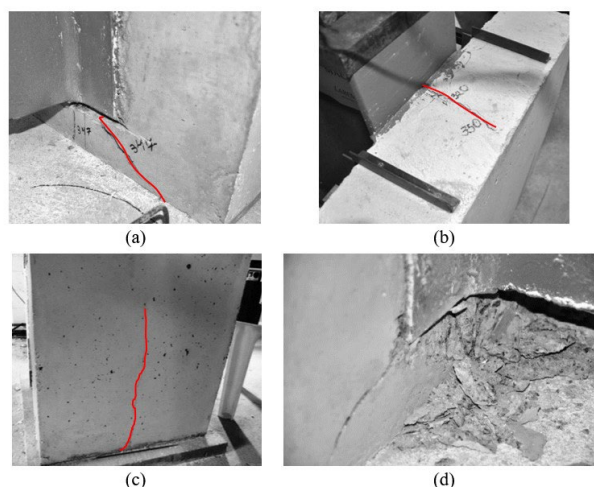


Figure 7. Cracking on MAC specimens. (a) failure at the concrete block; (b) cracks on the upper surface of the concrete slab; (c) longitudinal crack on the outer face of the slabs; (d) crushing of the concrete

Generally, the absence of cracking on the outer faces of MAC-1 and MAC-3 specimens, as well as the slight propagation of these existing cracks in MAC-2, should be due to the higher reinforcement ratio defined for the concrete slab's inner region, and because this face is further away from the region with the highest loading concentration. In this sense, the models presented a satisfactory behavior related to crack propagation.

After the push-out tests, an autopsy was performed on all the MAC specimens aiming to observe the various constituent parts, and it was observed that in all specimens, there was crushing of concrete in the region immediately below the connector (Figure 8). However, there was no sign of damage in the connector, showing that the failure occurred in the concrete slabs (Figure 9). The minor presence of concrete attached to the flange – Interface 2 – indicates that this interface had a lower contribution to the final resistance of the connection. Different from Interface 2, the presence of concrete attached to the linear connector's ribs (Figure 9a and Figure 9b) points out that Interface 1 (between between the concrete slab and the shear connector) probably contributed to a more significant proportion of the ultimate strength of the connection.

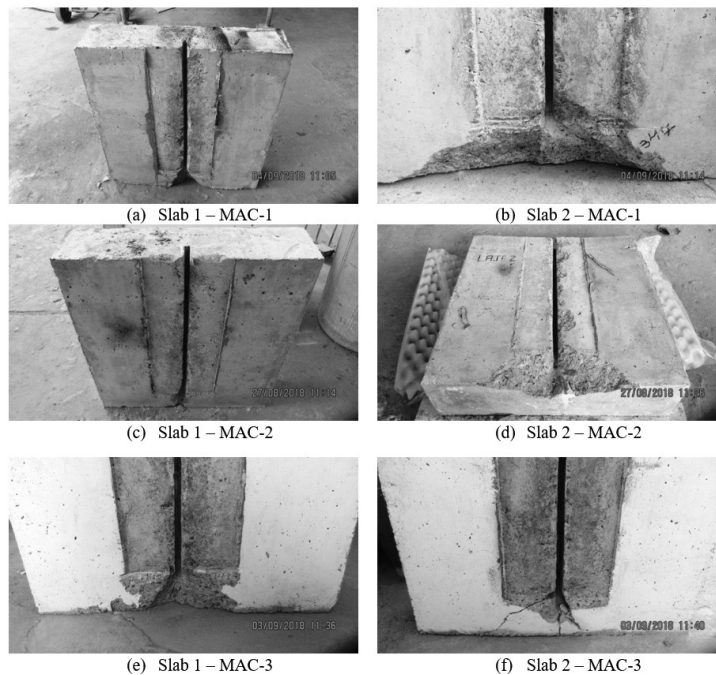


Figure 8. Autopsy of MAC specimens

Finally, Figure 9b shows the lower region of the connector, where it was noted that in all specimens the connectors presented the same straight geometry that they had before loading. On the other hand, the concrete area that was in contact with the front of the shear connector is heavily crushed. These observations indicate that the concrete strength, as well as the presence of the concrete end-bearing zone, were dominant factors in the connection behavior, and the failure of the specimens was conditioned by the concrete slabs.

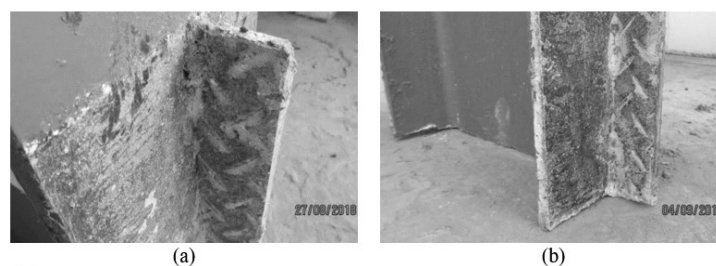


Figure 9. Final condition of the connectors (a) and (b) Details of the connector surface

2.4.4 TREL specimens

Specimens TREL-1 and TREL-2 presented the first cracks at around 61% and 76% of the maximum load capacity. In TREL-1 specimen, cracks initially appeared simultaneously on the outer face of both slabs (Figure 10a and Figure 10b), while in TREL-2 they appeared on slab 2, in the region near the connector at the top of the slab, as well as on the interior area in the zone that is located immediately below the connector, as represented by Figure 10c. Cracking occurred earlier in TREL specimens, when comparing to MAC specimens, due to the arrangement of the concrete section: they present a lower ratio of reinforcement and less concrete mass (see section 2.1).

When TREL-1 reached 253.4 kN, the specimen presented a small asymmetry since the slip recorded in slab 1 was higher than the slip recorded in slab 2. Afterwards, cracks appeared in the inner region of both slabs on specimen TREL-1 for a load of 290.0 kN. For this load level, it was possible to verify the propagation of the longitudinal crack already present on the outer face of slab 1. Before the maximum load, another crack was identified at the top of slab 1, near the alignment of the connector (Figure 10d). A maximum load of 409.2 kN was registered, for this specimen, associated with the sudden failure of slab 1. Figure 10f represents the behavior reported, i.e., one side of the specimen presented high slip values and the other side remained with small slip values until the end of the test.

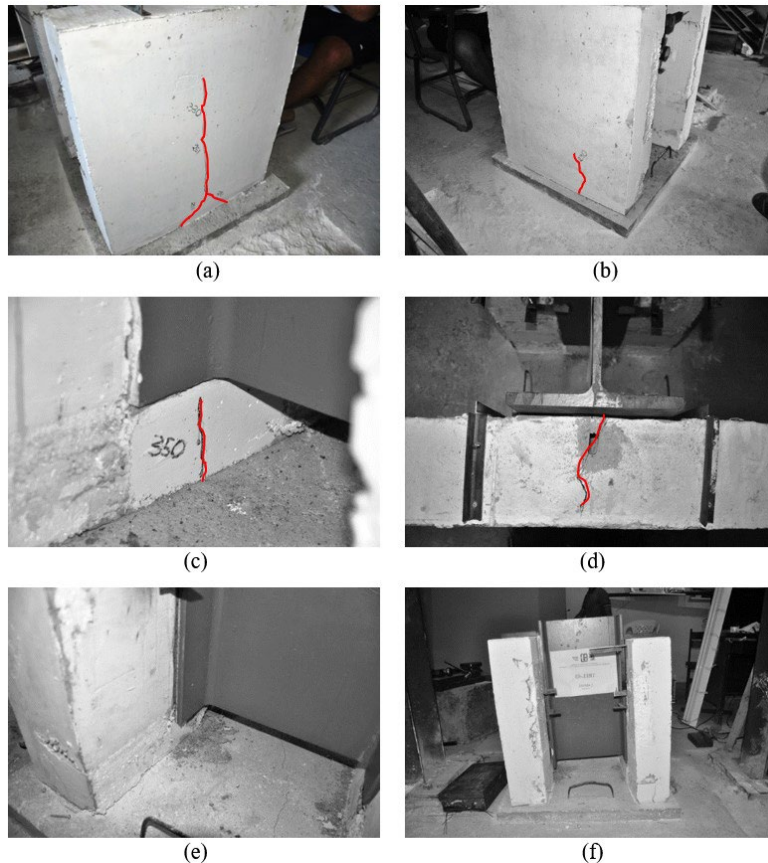


Figure 10. Cracking on TREL specimens. (a) and (b) longitudinal cracks on the outer surface; (c) under the connector; (d) at the top of the slab; (e) crushing on the concrete block; (f) asymmetric behavior of specimen TREL-3

As the load was increased, it was possible to observe the beginning of failure on Interface 2, before the maximum load is reached. Also, a higher propagation of existing cracks positioned in the top of the slabs, and a larger crushing of the inner bottom region of the concrete slab, were observed in TREL specimens (Figure 10d and Figure 10e), when these are compared to MAC specimens. All TREL specimens presented longitudinal cracks on the outer surface of the concrete slab, that evolved from bottom to top (see Figure 10a and Figure 10b). The same type of cracking was only seen on specimen MAC-2.

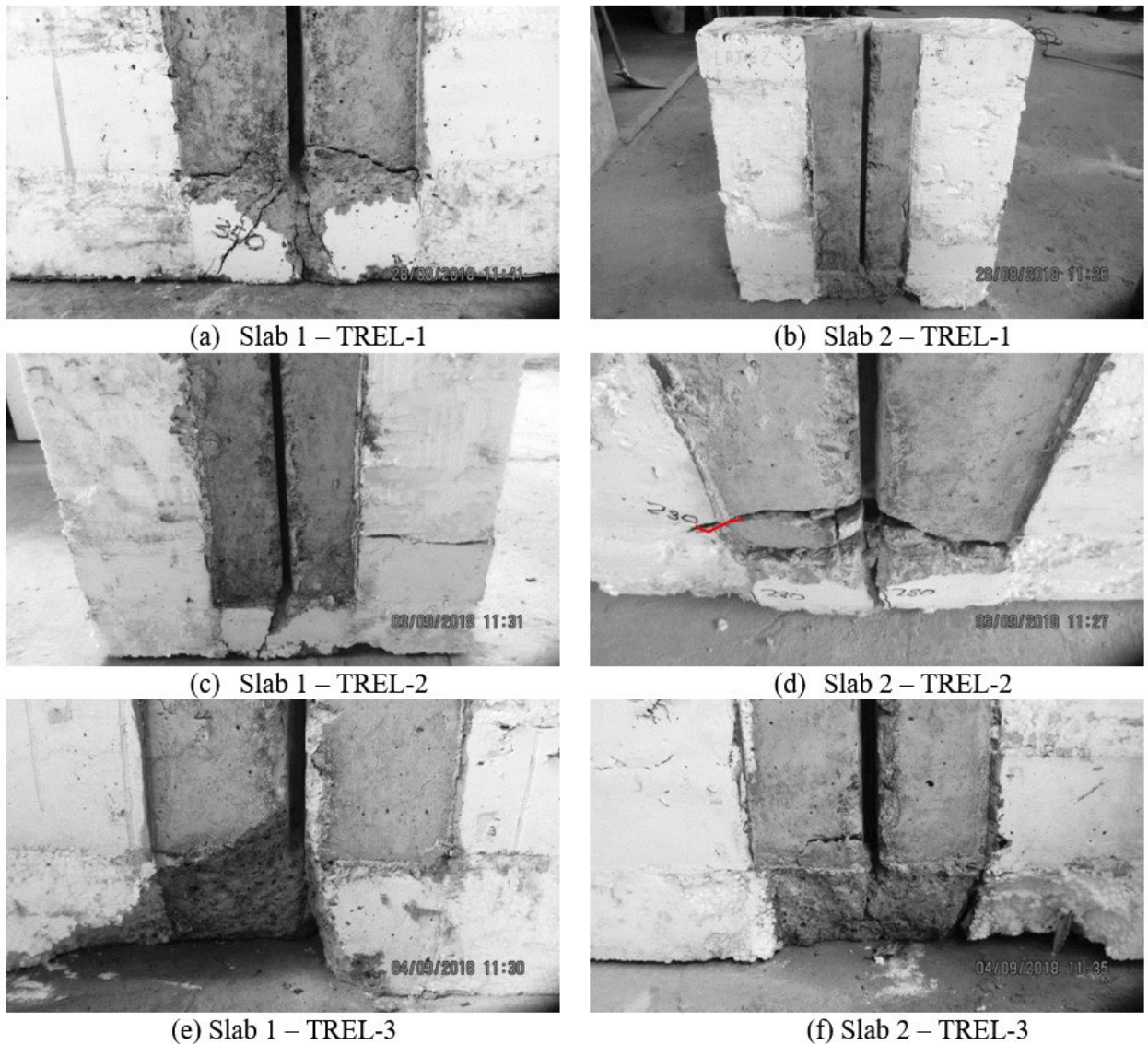


Figure 11. Autopsy of the TREL specimens

According to the autopsies performed, it was observed that in all the specimens, there was concrete crushing in the region immediately below the connector, similar to what happened in MAC specimens. In TREL-2, approximately horizontal cracks appeared in the lower region of slab 2 (Figure 11d). These cracks are different from the ones observed in MAC specimens, as they appear higher in the slab and cross the concrete rib created by the lattice joist at the lower part of the slabs. Naturally, TREL specimens present regions with a smaller effective flange width (b_f) in comparison to MAC specimens, which condition the formation of these cracks. TREL specimens presented a wider propagation of cracks on the outer face of the specimen's slabs, when compared to MAC specimens, and the formation of a horizontal crack aligned with the transition between plain concrete and the region with EPS block. The conditions presented by the connectors in TREL specimens were similar to those observed in MAC specimens (Figure 9), where Interface 1 (see Figure 2b) contributed mostly to the final resistance of the connection. However, the evolution of slip was generally more asymmetric between the two slabs of each TREL specimen than in MAC specimens.

The connectors maintained their geometrical characteristics intact, including in TREL-3. That indicates that the specimens' failure did not result from the response of the steel connector but rather from the concrete strength and the presence of concrete in front of the connector frontal edge.

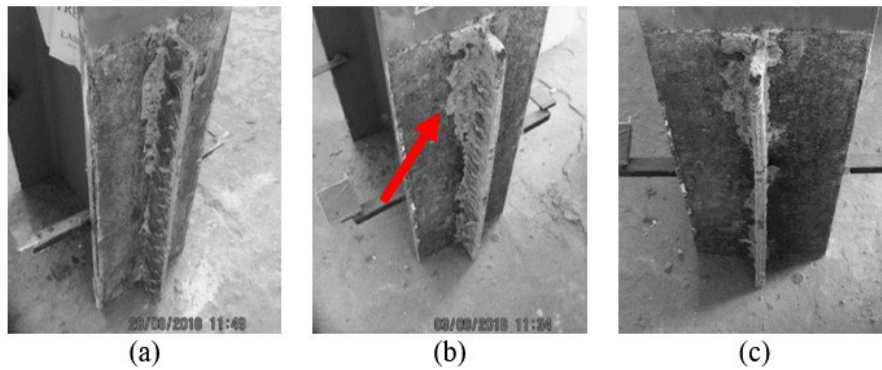


Figure 12. The final condition of the connectors – TREL specimens

2.4.5 Shear stiffness and ductility

Table 2 shows high shear stiffness values per connector (K_s). TREL specimens obtained an average stiffness value of 372.1 kN/mm, which represents just around 48% of what was achieved by MAC specimens ($K_s = 761.8$ kN/mm). Thus, it can be inferred that the connection by adherence in solid slabs tends to present higher initial shear stiffness than the connection by adherence in models with latticed joist slabs. Possibly, the transversal reinforcement area disposed on the slab's upper face of MAC and TREL specimens, which is $A_{s,MAC} = 2.51$ cm² and $A_{s,TREL} = 0.36$ cm², respectively, plays an important role in confining the specimen. The ratio between the transversal reinforcement area and the concrete area is 0.36% for MAC specimens (solid slab) and 0.07% for TREL models.

Ductility is another important index in reflecting the mechanical properties of shear connectors. It is defined by the slip δ_{uk} measured for the characteristic shear capacity P_{Rk} in the post-cracking branch. In Eurocode 4 [16], a minimum slip capacity of 6 mm is demanded to classify shear connectors as ductile. The Connection by Adherence for MAC specimens demonstrated a ductile behavior, since two models presented a δ_{uk} value in the order of 8 mm and one specimen presented a δ_{uk} value of 5.74 mm, which is close to the limit of 6 mm recommended by the Eurocode 4 [16]. On the opposite side, TREL specimens presented a general less ductile behavior, since two specimens presented a δ_{uk} value in close to 4 mm.

The ductility factor (D_c), which is given by the relation between δ_{uk} and δ_{Pmax} and is presented in Table 2, shows that the specimens with latticed joist slab presented an average ductility ratio equal to 2.14, which represents about 65% of that obtained by the specimens with solid slab. It can be inferred that TREL specimens have a lower ductility than MAC specimens. Some similar behavior concerning low ductility was obtained by Ahn et al. [25] in push-out tests with Perfobond shear connectors, as well [15], who performed tests with Perfobond and Connector by Adherence, and Kong et al. [26], who tested both Perfobond and Modified Clothoid (MCL) connectors (see Table 3 and Table 4).

2.4.6 Comparison with results obtained by other authors

A comparison is established between the load capacity obtained in the tests performed and the one calculated for commonly used connectors. The comparison is performed in terms of the mean value of the ultimate strength of each connector divided per linear meter of the interface (P_{lin}), which can be obtained by dividing the average maximum load (LC) by twice the length of the shear connector evaluated, which results in 358.5 kN/m for MAC specimens and 348.4 kN/m for TREL specimens.

In the research developed by Diógenes et al. [15], the interface that provides the higher resistance to connection by adherence was developed with high strength mortar (HPM), which indeed increased the maximum load capacity of the specimens. In this aspect, the specimens used by Diógenes et al. [15] were similar to those presented by Thomann and Lebet [14], as there was no concrete immediately below the connector, thus not mobilizing the frontal strength provided by the concrete volume that is positioned in front of the connector.

The load capacity in the specimen studied by Diógenes et al. [15] was similar to the one obtained by Papastergiou and Lebet [27] (see Table 3), which could be explained by the high resistance of the material and interfaces used. Even though the load capacity obtained in Diógenes et al. [15] and Papastergiou and Lebet [27] was higher, the characteristic slip values measured in the present research indicates a larger ductility of this type of connection, which is a very interesting result in

the scope of the application envisaged. It is believed that this increase in ductility is highly influenced by the concrete layer positioned in front of the connector, which was not present in the specimens tested by Diógenes et al. [15] or Papastergiou and Lebet [27]. In addition, according to the shear stresses, MAC and TREL models presented intermediate values to those of Papastergiou and Lebet [27] and Diógenes et al. [15], which certainly indicates the efficiency of this connection by adherence made with checkered steel plate.

Table 3. Results obtained with linear connectors.

Ref.	Type	Connector									
		L [mm]	H [mm]	T [mm]	A ^c [cm ²]	C _s [kg/m]	f _c [MPa]	P _{max} [kN]	P _{lin} [kN/m]	δ _{uk} [mm]	τ _{average} [MPa]
Diógenes et al. [15]	R_03	570	65	19	741	9.70	76.37 ^a 38.76 ^b	790.3	692.9	0.51	4.49
	R_04							566.9	497.3	0.14	
	R_09							620.3	544.1	0.45	
	R_10							685.2	608.1		
	Mean							585.6			
Papastergiou and Lebet [27]	PR100_1	1000	110	16	2200	13.83	94.70 ^a C50/60 ^b	1269.0	634.5	3.32	2.88
	MAC-1	550	50	9.5	550	3.73	30.40 ^b	359.1	326.4	5.47	3.57
	MAC-2							417.2	379.3	7.90	
	MAC-3							404.3	367.5	8.41	
	TREL-1							409.2	372.0	7.00	
	TREL-2							357.2	324.7	4.01	
	TREL-3	271.8 ^d	247.1 ^d	3.94 ^d							
	Mean							354.0			

^a Compressive strength of the high strength mortar (HPM) present at the interface with the connector. ^b Compressive strength of the concrete of the specimens. ^c Regarding the area on both sides of the connector. ^d Value not considered

The steel consumption is analyzed in Table 3. The steel consumption (C_s) of connector by adherence from this research is 3.73 kg/m. Comparing the present study to other studies with similar connectors, Diógenes et al. [15] and Papastergiou and Lebet [27], a significant reduction in C_s is observed. Nevertheless, looking at C_s alone can lead to wrong conclusions. The increase of section inertia, changes the ratio between the span and the height of the steel profile, possibly culminating in an overall reduction in C_s. In the future, other parameters should be included in this discussion, for example, consumption of welding and man-hour. With the ratio of steel consumption (C_s) to the linear resistance per meter of connector (P_{lin}), it is possible to understand how much steel is associated with each unit of shear resistance (1 kN).

Connection by adherence presented and studied by Papastergiou and Lebet [27] seems quite promising. Their proposal demands a ratio of 22 g/1 kN. Looking for a practical, economical, and fast solution for connections in steel and concrete composite structures Diógenes et al. [15] presented a model whose ratio was 16 g/1 kN. The proposed connection by adherence with checkered steel plate presents an even lower demand for steel in the present work, with a ratio of 10 g/1 kN. Thus, it is believed that this is a potential alternative in the use of shear connectors on steel-concrete composite structures.

In Table 4, a comparison is established between the load capacity and shear stiffness values per connector obtained with the connector by adherence in MAC and TREL specimens and the corresponding results obtained by other types of shear connectors. It should be noted that the connectors shear stiffness was calculated according to section 2.4, where K_s is the slope of the line between the origin and P_{Rd} on load slip curves, except for stud connectors whose shear stiffness is defined as the secant modulus at the point where the applied load is half of the ultimate load on the load-slip curve for usually welded studs, as presented in He et al. [29]. This researcher investigated the shear stiffness of headed studs embedded in various types of concrete (NC, HPC, UHPC etc.), using a total of 206 push-out tests collected from the literature.

The results obtained by Diógenes et al. [15] (Table 3) show a high shear stiffness that probably results from the use of a high-performance mortar (HPM). The same behavior was observed by Papastergiou and Lebet [27]. Stud connectors have lower initial stiffness than that obtained by other types of connectors, such as Connector by Adherence, Perfobond, and MCL shear connector. The stiffness (K_s) of MAC specimens showed similar to Perfobond connectors, while TREL specimens similar to headed studs. Comparing MAC and TREL specimens, MAC presented a stiffness twice higher than TREL specimens.

Table 4. Load capacity and Stiffness per connector – different types.

Ref.	Type of connector	$P_{max}/connector$ – Average [kN]	K_s – Average [kN/mm]
MAC	Connector by adherence	196.8	761.8
TREL		191.6	372.1
Diógenes et al. [15]	Connector by adherence	332.8	17153.0
	Perfobond	367.4	13362.7
Kong et al. [26]	Perfobond	535.8	739.9
	MCL	418.9	614.1
Yang et al. [28]	Studs SN30	330.0	554.0

So, it is concluded that the connector proposed in this research show high load capacity and improved ductility. On average, the connection by adherence proposed presents a ductile behavior, which enables an adequate capacity of transmission of forces from the steel beam to the concrete slab.

3 NUMERICAL AND PARAMETRIC ANALYSES

3.1 FEM analysis overview

To complement and expand the experimental analysis, finite element modeling was conducted using ABAQUS *Simulia* [30]. First, a calibration analysis was performed to find the connection parameters which better describe the experimental results. Later, a comparison between the FEM calibrated and experimental models was made to discuss the feasibility of experimental results. A parametrical study was also developed, expanding the experimental discussion.

3.2 FE model description

A 3D solid model employing an 8-node linear brick element with reduced integration (C3D8R) was used for the concrete slab, the steel profile and the shear connector. The reinforcement bars were modeled using the embedded element technique. The connection by adherence was modeled using the general contact interaction procedure. The overall maximum mesh size adopted was 20 mm. The mesh size was analyzed, varying from 1 mm to 30 mm. About the boundary conditions, the nodal vertical displacements at the bottom of the concrete slabs were fully constrained, simulating the condition of slabs at the experimental test. The models were built in full without considering symmetry for both experimental samples, MAC and TREL types (Figure 13).

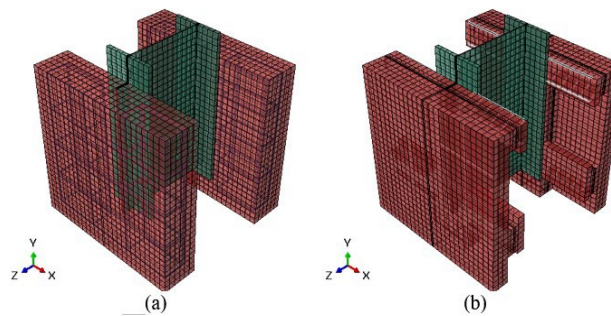


Figure 13. (a) MAC – FE model; (b) TREL – FE model

To perform a nonlinear structural analysis, a prescribed descending displacement was applied at the top of the steel profile, considering successive increments of 0.01 mm. The solution strategy used was the ABAQUS® *Simulia* default [30], considering the direct method and the “Full Newton” technique.

The concrete and steel mechanical properties adopted are described in Table 1. A reduction of 20% in the concrete dynamic elasticity modulus was made to determine the static elasticity modulus according to Diógenes et al. [31].

About the nonlinear behavior of concrete, the recommendations from Hafezolzghorani et al. [32] and CEB-FIP [33] were considering the adoption of the Plasticity Damage Model available in Abaqus. The yield stress and inelastic strain of concrete for both elastic and inelastic behavior (compressive and tensile behavior) was calibrated according to Hafezolzghorani et al. [32].

For all the steel materials was used an isotropic plasticity with initial modulus of Elasticity and yield stress according to Table 1. In addition, was used Density of 7850 kg/m³ and the Poisson’s ratio of $\nu = 0.3$ for both shear’s connectors and reinforcement bars. Parameters of ductile damage initiation criterions and damage evolution laws were derived observing basic behavior of tensile test coupons and implementing principles of progressive damage model described in ABAQUS Documentation [30].

The shear connection is defined using an interface with the Coulomb friction model. This model relates the maximum allowable frictional (shear) stress across an interface with the contact pressure between the contacting bodies. In the basic form of the Coulomb friction model, two contacting surfaces can carry shear stresses up to a certain magnitude across their interface before they start sliding relative to one another; this state is known as sticking” [30]. This model was chosen because it best described the interface behavior observed in the experimental stage. The friction coefficient used in the “Tangential Behavior” was initially defined based on the results obtained by Thomann [34], equal to 0.72, and was afterwards calibrated until the best fit between the numerical and the experimental curve was attained. As a result, the friction coefficient calibrated was 0.8.

Concerning stiffness (tangential, normal, and transverse) in the cohesive behavior, more focus was given to the tangential cohesive behavior (K_{tt}), by considering this parameter's calibration, obtained through shear stress versus slip curve. Values close to zero were admitted for normal and transverse stiffness. Finally, the values of K_{tt} = 2.1 MPa/mm for MAC specimens and a K_{tt} = 1.0 MPa/mm for TREL specimens were adopted. Table 5 summarizes all the FE parameters calibrated to enable the interface that simulates the connection.

Table 5. Calibrated interface parameters used in the FE model

Coulomb friction model parameters		MAC	TREL	
INTERFACE	Tangential Behavior	Coefficient of friction	0.8	0.8
		Friction Formulation	Penalty	Penalty
		Shear stress	No limit	No limit
	Normal Behavior	Pressure - Overclosure	Hard Contact	Hard Contact
	Cohesive Behavior	K _{tt} (MPa/ mm)	2.1	1.0
K _{nn} and K _{ss} (MPa/ mm)		10e ⁻⁶	10e ⁻⁶	
Damage	Type/Softening	Displ. Exponential	Displ. Exponential	

3.3 FE model x Experimental Model

Numerical force–slip curves of complete FE models of MAC and TREL specimens are compared, in Figure 14, with representative experimental load–slip curves for loading up to failure. The numerical results obtained on FE models show a good agreement with the experimental ones. The numerical models are used for failure modes identification and further parametric analysis.

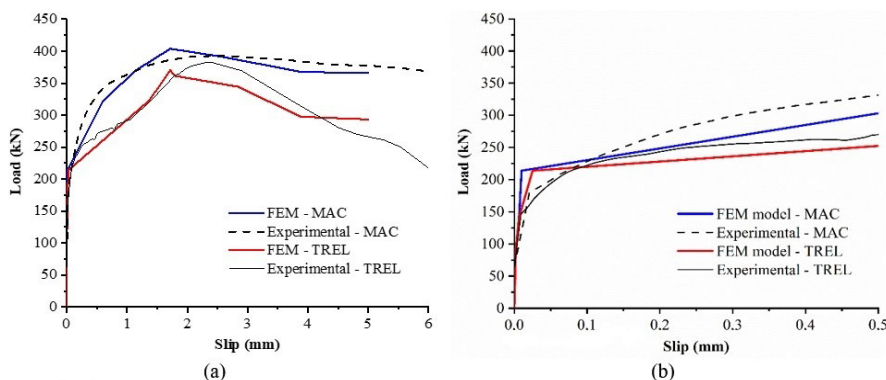


Figure 14. Experimental and FE force–slip curves, (a) General Force-slip curves, (b) Curve Initial brand

Figure 15 shows the stresses measured on the concrete slabs when the maximum load is applied, respectively, on MAC and TREL FE models. A concentration of stresses at the bottom of the slabs is observed. This behavior is coherent with the specimens' experimental observations regarding the cracking aspect and deformed shape (see Figure 8, Figure 9 and Figure 16a for MAC specimens and Figure 11, Figure 12 and Figure 16b for TREL specimens). In the MAC model, a high-stress concentration is visible in the inner concrete slabs' side, around the bottom of the shear connector, and in TREL model, these high stresses are spread in the block of bulk concrete positioned under the connector (Figure 15a and Figure 15b). There are tensile stresses in the concrete slabs' outer faces, and these are higher on the lower parts, both for MAC and TREL models. The level of tensile stress is similar for MAC and TREL in the outer faces of the slabs, indicating tensile stress upper to its concrete's resistance (Figure 15c and Figure 15d). No significant level of tensile stresses was presented by the profile and connector in the FE models, indicating also a stress level smaller than yield strength for both elements (Figure 15e and Figure 15f), similar to the behavior presented in Figure 9 and Figure 12, where no significant deformation related to plasticization was observed.

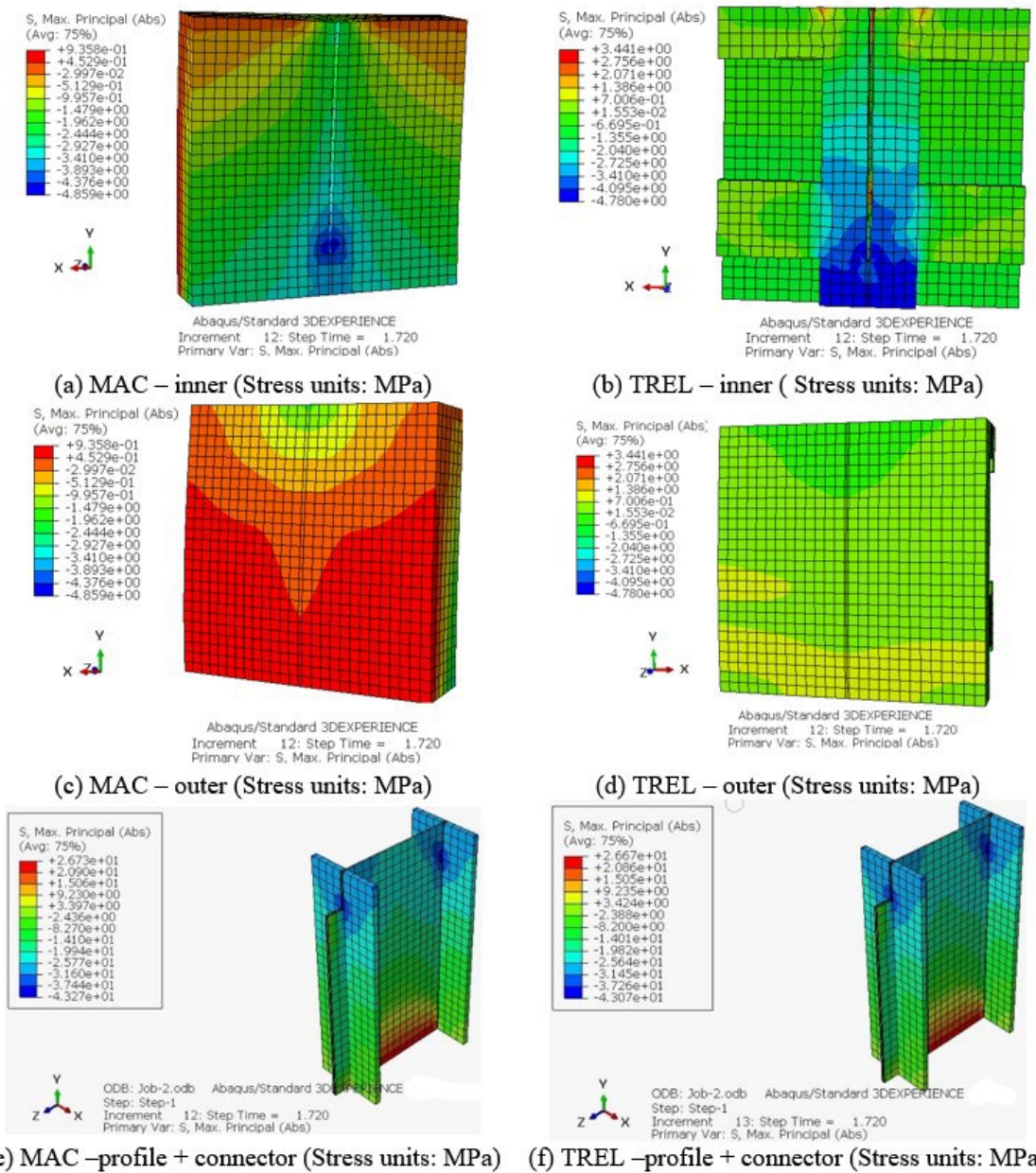


Figure 15 Distribution of principal stresses on the FE models (MPa): (a,c,e) MAC; (b,d,f) TREL

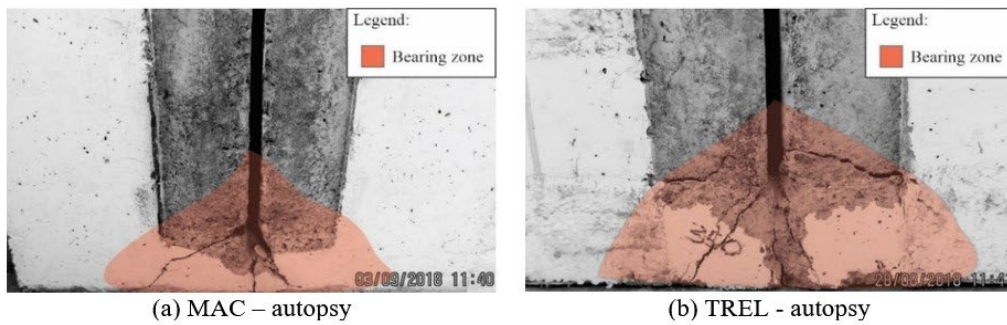


Figure 16. Failure modes of the specimens: (a) MAC; (b) TREL

3.4 Parametric FEM analysis

A parametric study is presented to investigate how the variation in the concrete's strength, in the connector's height, in the connector's length and in the connector's thickness affects the FE models developed. The concrete grades analyzed were C20 and C40. In general, no significant differences were observed between de analyzed grades C20, C30, and C40 for MAC models. This means that the load capacity of MAC specimens depends mostly on the shear stresses developed on the steel-concrete interfaces and less on the end bearing effect provided by the concrete slab in the bottom of shear connector. For TREL models, comparing the C30 grade models with the others shows that a 10 MPa increase in the concrete's strength caused a load capacity gain of around 6.0% while decreasing this value provoked a loss around 3.7% on capacity.

The concrete quality influence on the behavior of push-out models was also investigated numerically by Diógenes [35]. Before the numerical stage, experimental analyses were conducted to a concrete grade around 40 MPa and considering the R and RP interfaces (Figure 1a and Figure 1d) in addition to the L interface without ribs. Based on the results, it was possible to observe that the rupture was controlled by the interface, indicating that the concrete's quality should not significantly influence the numerical model. Despite this, a parametric analysis was carried out to investigate the behavior of prototypes with f_c equal to 60 and 20 MPa, and for the L, R and RP interfaces. For the C60-concrete, increases of 5.6%, 16.11% and 19.21% were obtained, respectively and C20-concrete, decreases of 8.9%, 5.5%, and 4.3% were obtained, respectively. The results obtained in this work agree with what was presented by Diógenes [35].

Because these results to concrete variation were not significant, only the effects of the variation on connector's parameters are showed in Figures 17 to 19.

3.4.1 Connector height

It was observed that the increase in the connector's height caused a gain of 25% in load capacity for MAC models and 16% in the load capacity for TREL models (Figure 17).

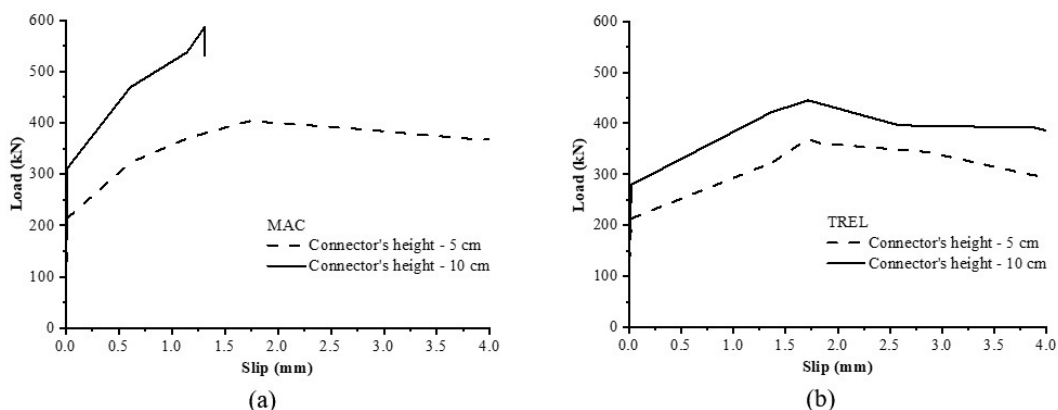


Figure 17. FEA force-slip curves for different connector's height: (a) MAC; (b) TREL

The increase in the connector’s height causes higher stress levels in the concrete slabs, which is consistent with the increase in the models’ load capacity. In general, the increase in the connector’s height had a higher influence on the connection load capacity than the increase in the concrete’s strength.

3.4.2 Connector’s length

As shown in Figure 18, the increase in the connector’s length caused a gain of 28% in load capacity for MAC specimens and 30% in the load capacity for TREL specimens. Parallely, the slip capacity increased by 21% for MAC specimens, unlike the TREL specimens which the slip capacity decreased by about 33% when the connector length was two times greater.

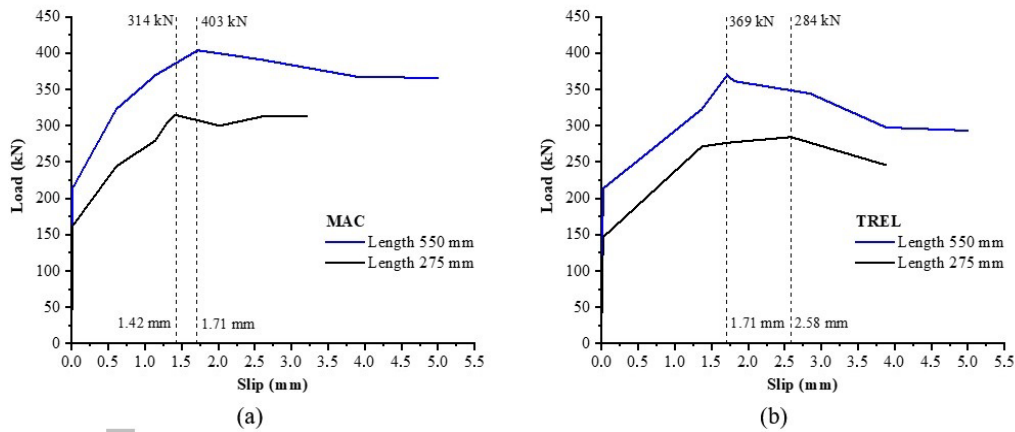


Figure 18 FEA force–slip curves for different connector’s length: (a) MAC; (b) TREL

These results can be related to the decrease in the connector’s area that contributed to the model resistance. The decrease in half of the connector’s area did not proportional to the decreased load capacity in either of the studied models. In general, the increase in the connector’s height, and the decrease in the connector’s length had a higher influence on the connection load capacity than the increase in the concrete’s strength.

3.4.3 Connector’s thickness

It was observed that the decrease in the connector’s thickness from 9.75 mm to 6.00 mm caused a gain of 1.30% in load capacity for MAC models and 1.42% in the load capacity for TREL models (Figure 19). This increase in the connector’s thickness from 9.75 mm to 12.6 mm caused a loss of 23.7% in load capacity for MAC models and 19.7% in the load capacity for TREL models. Still, was noted a brittle rupture in models with a connector thickness of 12.6 mm.

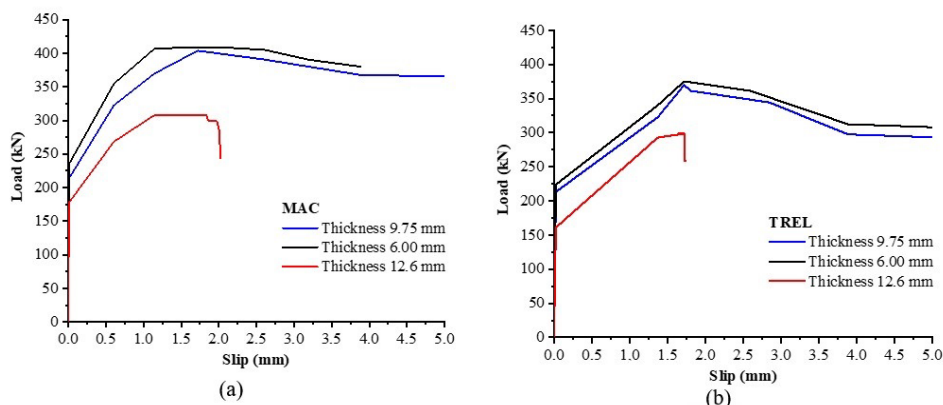


Figure 19. FEA force–slip curves for different connector’s thickness: (a) MAC; (b) TREL

These results are associated with a higher stress concentration in the slabs, damaging the slab more sharply. Finally, the increase in the connector's height, and the decrease in the connector's length had a higher influence on the connection load capacity than the increase in the concrete's strength or the variation in the connector's thickness.

4 CONCLUSIONS

This paper discussed an innovative technology for connection by adherence, whose resistance is due to friction on various steel-concrete interfaces. This type of shear connection is suitable for composite beams with latticed joists slabs, and the paper intended to analyze the behavior of the proposed connection, in this application's context, through experimental and numerical approaches. The following conclusions are summarized: 1) The connection failure is related to slip at Interface 1 (see Figure 2b), where crack formation and propagation develop with increasing load, followed by crushing of concrete in the region immediately below the connector; 2) In all specimens, the slabs suffered concrete cracking and crushing in the region immediately below the connectors. The connectors remained intact at the end of the tests. In this way, the failure of all the models, is mainly associated with the failure of the concrete slabs; 3) The interface between the shear connector and the concrete slab (see Interface 1 represented in Figure 2b) was the one that most contributed to the connection load capacity; 4) By comparison with the experimental results obtained in this work, it is observed that in the interfaces involved in connections by adherence associated with high-performance mortar (HPM), the shear stiffness increases significantly; 5) The specimens with latticed joist slabs were more prone to cracking since they had less transversal reinforcement and less concrete area when compared to solid slabs; 6) TREL specimens presented average load capacity values with the same magnitude of the obtained in models with reinforced concrete slabs; 7) Although MAC and TREL specimens had similar strength, there were differences in the slip values measured. TREL specimens presented a worse behavior because after reaching the maximum load, they suffered a faster drop of load capacity and developed smaller values of slip; 8) Specimens with prefabricated slabs (TREL) suffered higher uplift than specimens with solid reinforced slabs (MAC); 9) The existence of an end-bearing concrete zone in the specimens indeed increased the initial shear stiffness; 10) The FE calibration demonstrated the consistency of the experimental results and allowed to perform some variations related to concrete strength, connector's length, thickness, and the connector's height. This last variation had the highest influence on load capacity; 11) Finally, it is possible to indicate that the connector by adherence made with a checkered steel plate proposed, exhibited good strength and ductility.

ACKNOWLEDGEMENTS

To the MIMEE – UFPB Laboratory group. To the Coordination for the Improvement of Higher Education Personnel (CAPES) and the National Council for Scientific and Technological Development (CNPq). In addition to Gerda S.A and J.C. Metallurgy, for the donation of RC steel bars and metal profiles, respectively

REFERENCES

- [1] K. Benyahi, Y. Bouafia, M. Oudjene, S. Barboura, and M. S. Kachi, "Numerical procedure for the three-dimensional nonlinear modelling of composite steel-concrete beams," *Int. J. Steel Struct.*, vol. 21, no. 3, pp. 1063–1081, 2021, <http://dx.doi.org/10.1007/s13296-021-00490-1>.
- [2] D. Wang, B. Tan, L. Wang, F. Chen, and S. Xiang, "Numerical study on stress intensity factors for stud connectors of steel-concrete connection," *Int. J. Steel Struct.*, vol. 21, no. 5, pp. 1775–1789, Oct 2021, <http://dx.doi.org/10.1007/s13296-021-00534-6>.
- [3] I. B. Valente and P. C. Cruz, "Experimental analysis of shear connection between steel and lightweight concrete," *J. Construct. Steel Res.*, vol. 65, no. 10–11, pp. 1954–1963, 2009, <http://dx.doi.org/10.1016/j.jcsr.2009.06.001>.
- [4] D. Papastergiou and J.-P. Lebet, "Design and experimental verification of an innovative steel-concrete composite beam," *J. Construct. Steel Res.*, vol. 93, pp. 9–19, 2014, <http://dx.doi.org/10.1016/j.jcsr.2013.10.017>.
- [5] L. Bouazaoui, B. Jurkiewicz, Y. Delmas, and A. Li, "Static behaviour of a full-scale steel-concrete beam with epoxy-bonding connection," *Eng. Struct.*, vol. 30, no. 7, pp. 1981–1990, 2008, <http://dx.doi.org/10.1016/j.engstruct.2007.12.018>.
- [6] M. Thomann and J. P. Lebet, "Design method for connections by adherence for steel concrete composite bridges," *Struct. Eng. Int.*, vol. 17, no. 1, pp. 86–93, 2007, <http://dx.doi.org/10.2749/10168660779938778>.
- [7] A. R. Alves, M. I. B. Valente, W. B. Vieira, and G. S. Veríssimo, "Prospective study on the behaviour of composite beams with an indented shear connector," *J. Construct. Steel Res.*, vol. 148, pp. 508–524, 2018, <http://dx.doi.org/10.1016/j.jcsr.2018.06.015>.
- [8] J. P. S. Cândido-Martins, L. F. Costa-Neves, and P. C. G. S. Vellasco, "Experimental evaluation of the structural response of Perfobond shear connectors," *Eng. Struct.*, vol. 32, no. 8, pp. 1976–1985, 2010, <http://dx.doi.org/10.1016/j.engstruct.2010.02.031>.

- [9] E. C. Oguejiofor and M. U. Hosain, "A parametric study of perfobond rib shear connectors," *Can. J. Civ. Eng.*, vol. 21, no. 4, pp. 617–624, 1994, <http://dx.doi.org/10.1139/194-063>.
- [10] A. L. Camargo, J. P. C. Rodrigues, R. H. Fakury, and L. Laim, "Fire resistance of axially and rotationally restrained concrete-filled double-skin and double-tube hollow steel columns," *J. Struct. Eng.*, vol. 145, no. 11, pp. 04019128, 2019, [http://dx.doi.org/10.1061/\(ASCE\)ST.1943-541X.0002428](http://dx.doi.org/10.1061/(ASCE)ST.1943-541X.0002428).
- [11] I. Valente and P. J. S. Cruz, "Experimental analysis of Perfobond shear connection between steel and lightweight concrete," *J. Construct. Steel Res.*, vol. 60, no. 3–5, pp. 465–479, 2004, [http://dx.doi.org/10.1016/S0143-974X\(03\)00124-X](http://dx.doi.org/10.1016/S0143-974X(03)00124-X).
- [12] J. C. Vianna, S. A. L. Andrade, P. C. G. Vellasco, and L. F. Costa-Neves, "Experimental study of Perfobond shear connectors in composite construction," *J. Construct. Steel Res.*, vol. 81, pp. 62–75, 2013, <http://dx.doi.org/10.1016/j.jcsr.2012.11.002>.
- [13] Y. Liu, H. Xin, and Y. Liu, "Experimental and analytical study and tensile performance of perfobond connector in bridge engineering application," *Structures*, vol. 2021, no. 4, pp. 714–729, 2021, <http://dx.doi.org/10.1016/j.istruc.2020.11.045>.
- [14] M. Thomann and J. P. Lebet, "The modelling of an embossed steel-to-cement paste confined interface loaded in shear," *J. Construct. Steel Res.*, vol. 63, no. 5, pp. 639–646, May 2007, <http://dx.doi.org/10.1016/j.jcsr.2006.06.038>.
- [15] H. J. F. Diógenes, A. L. H. C. El Debs, and I. B. Valente, "Experimental analysis of new interfaces for connections by adhesion, interlocking and friction," *J. Construct. Steel Res.*, vol. 110, pp. 170–181, Jul 2015, <http://dx.doi.org/10.1016/j.jcsr.2015.03.012>.
- [16] European Standard, *Eurocode 4: Design of Composite Steel and Concrete Structures-Part 1-1: General Rules and Rules for Buildings*, 2004.
- [17] Associação Brasileira de Normas Técnicas, *Concreto – Ensaio de Compressão de Corpos de Prova Cilíndricos*, ABNT NBR 5739, 2018.
- [18] American Society for Testing and Materials, *Standard Test Method for Fundamental Transverse, Longitudinal, and Torsional Resonant Frequencies of Concrete Specimens*, ASTM-C215-08, 2008.
- [19] Associação Brasileira de Normas Técnicas, *Materiais Metálicos – Ensaio de Tração à Temperatura Ambiente*, ABNT NBR 6152, 2002.
- [20] H. J. F. Diógenes, A. L. H. C. El Debs, and I. B. Valente, "Tests on composite beams using new connections by adherence," *Proc. Inst. Civ. Eng., Struct. Build.*, vol. 171, no. 2, pp. 149–165, Feb 2018, <http://dx.doi.org/10.1680/jstbu.16.00175>.
- [21] S.-H. Kim, K.-T. Choi, S.-J. Park, S.-M. Park, and C.-Y. Jung, "Experimental shear resistance evaluation of Y-type perfobond rib shear connector," *J. Construct. Steel Res.*, vol. 82, pp. 1–18, Mar 2013, <http://dx.doi.org/10.1016/j.jcsr.2012.12.001>.
- [22] H.-Y. Kim and Y.-J. Jeong, "Experimental investigation on behaviour of steel-concrete composite bridge decks with perfobond ribs," *J. Construct. Steel Res.*, vol. 62, no. 5, pp. 463–471, May 2006, <http://dx.doi.org/10.1016/j.jcsr.2005.08.010>.
- [23] Y.-J. Jeong, H.-Y. Kim, and H.-B. Koo, "Longitudinal shear resistance of steel–concrete composite slabs with perfobond shear connectors," *J. Construct. Steel Res.*, vol. 65, no. 1, pp. 81–88, Jan 2009, <http://dx.doi.org/10.1016/j.jcsr.2008.01.031>.
- [24] I. B. Valente and P. J. S. Cruz, "Experimental analysis of shear connection between steel and lightweight concrete," *J. Construct. Steel Res.*, vol. 65, no. 10–11, pp. 1954–1963, Oct 2009, <http://dx.doi.org/10.1016/j.jcsr.2009.06.001>.
- [25] J.-H. Ahn, C.-G. Lee, J.-H. Won, and S.-H. Kim, "Shear resistance of the perfobond-rib shear connector depending on concrete strength and rib arrangement," *J. Construct. Steel Res.*, vol. 66, no. 10, pp. 1295–1307, Oct 2010, <http://dx.doi.org/10.1016/j.jcsr.2010.04.008>.
- [26] F. Kong, P. Huang, B. Han, X. Wang, and C. Liu, "Experimental study on behavior of corrugated steel-concrete composite bridge decks with MCL shape composite dowels," *Eng. Struct.*, vol. 227, pp. 111399, Jan 2021, <http://dx.doi.org/10.1016/j.engstruct.2020.111399>.
- [27] D. Papastergiou and J.-P. Lebet, "New steel-concrete connection for prefabricated composite bridges," *Stahlbau*, vol. 80, no. 12, pp. 894–903, 2011., <http://dx.doi.org/10.1002/stab.201101493>.
- [28] F. Yang, Y. Liu, and Y. Li, "Push-out tests on large diameter and high strength welded stud connectors," *Adv. Civ. Eng.*, vol. 2018, pp. 1–12, Sep 2018, <http://dx.doi.org/10.1155/2018/4780759>.
- [29] J. He, Y. Lin, Y. Liu, X. Xu, H. Xin, and S. Wang, "Shear stiffness of headed studs on structural behaviors of steel-concrete composite girders," *Steel Compos. Struct.*, vol. 36, no. 5, pp. 553–568, 2020.
- [30] SIMULIA, *ABAQUS Documentation*. Providence, RI, USA, 2011.
- [31] H. J. F. Diógenes, L. C. Cossolino, A. H. A. Pereira, M. K. El Debs, and A. L. H. C. El Debs, "Determinação do módulo de elasticidade do concreto a partir da resposta acústica," *Rev. IBRACON Estrut. Mater.*, vol. 4, no. 5, pp. 792–813, 2011.
- [32] M. Hafezolzhorani, F. Hejazi, R. Vaghei, M. S. Bin Jaafar, and K. Karimzade "Simplified damage plasticity model for concrete", em *Structural Engineering International*, Int. Assoc. for Bridge and Structural Eng. Eth-Honggerberg, fev. 2017, p. 68–78. doi: <http://dx.doi.org/10.2749/101686616X1081>.
- [33] Comité Euro-International Du Béton, *CEB-FIP Model Code 1990. Vol. 1993*. Thomas Telford Publ., 1990.
- [34] M. Thomann, *Connexions par Adhérence Pour les Ponts Mixtes Acier-Bétoni*. Lausanne: Ec. Polytech. Fed. Lausanne, 2005.
- [35] H. J. F. Diógenes, "Análise numérica e experimental de ligações por aderência aço - concreto aplicada em estruturas mistas," Ph.D. dissertation, Univ. São Carlos, São Carlos, 2013.

Author contributions: All authors contributed to the study conception and design. Material preparation, data collection and analysis were performed by Lisarb H Brasil, Hidelbrando J F Diógenes, Maria Isabel B Valente e Lays R A da Costa. The first draft of the manuscript was written by Lisarb H Brasil e Lays R Az da Costa and all authors commented on previous versions of the manuscript. All authors read and approved the final manuscript.

Editors: Ricardo Carrazedo, Guilherme Aris Parsekian.